Journal of Catalysis **187,** 385–391 (1999)
Article ID jcat.1999.2607, available online at http://www.idealibrary.com on IDEAL®

New Catalysts Active for the Mild Oxidation of Hydrogen Sulfide to Sulfur

E. Laperdrix,* G. Costentin,[1] N. N Guyen,† O. Saur,* and J. C. Lavalley*

*Laboratoire Catalyse et Spectrochimie and †Laboratoire CRISMAT, ISMRA, 6 Boulevard Maréchal Juin, 14050 Caen Cedex, France

Received March 1, 1999; revised June 18, 1999; accepted June 20, 1999

Nickel iron phosphates were studied for the selective oxidation of hydrogen sulfide to sulfur. Nickel iron phosphate and Fe/Cr samples were more active than simple iron, chromium, and mixed iron–chromium oxides, which had been previously studied. Nickel iron phosphate catalyst prepared by solid–solid method with, consequently, a very low specific surface area was intrinsically active and selective to sulfur (conversion 17%, S_n selectivity 97%); no rapid deactivation was observed. Even though higher specific surface area samples, prepared according to a solution method at various calcination temperatures, showed better performance (conversion 76%, S_n selectivity >90%), the specific activity depended on the crystallinity of the samples. The reaction is apparently structure sensitive. The structure of the catalytic material must facilitate electronic exchange, evidenced by Mössbauer Characterization. The establishment of the mixed valency Fe^{2+}/Fe^{3+} under catalytic feed was shown to be an essential factor in this reaction.

INTRODUCTION

Most hydrogen sulfide is removed from industrial waste gases via the Claus process (1). Since the catalytic step in this process is an equilibrium,

$$2H_2S + SO_2 \leftrightharpoons 3/nS_n + 2H_2O,$$

the transformation of H_2S is incomplete and about 3% of the remaining H_2S still must be transformed. One proposal is the mild oxidation of hydrogen sulfide to elementary sulfur. This reaction is particularly convenient for selectively oxidizing small amounts of H_2S to sulfur. The most important aim is to obtain very good selectivity in sulfur, the remaining H_2S being recyclable. Thus, SO_2 formation must be avoided.

In the Superclaus process (2), H_2S is oxidized directly by O_2 at 230°C. It is claimed that catalysts based on mixed iron–chromium oxides, deposited on α-Al_2O_3, are quite effective (3). This support has a lower specific area and larger pores than γ-Al_2O_3, thus minimizing the likelihood of the retro-Claus reaction and the oxidation of elemental sulfur to SO_2. The importance of chromium has also been stressed; it favors S_n selectivity. Moreover, the presence of chromium improved the resistance of the catalyst to deactivation. The Fe^{2+}/Fe^{3+} mixed valency is supposed to play an important role, with $FeSO_4$ being the active phase, although this has not been proven.

Because of the toxicity of chromium, a second generation of catalysts, based on Fe_2O_3 deposited on silica, has been developed. However, the stability of the industrially used catalyst remains poor (4). Moreover, its selectivity to sulfur is still lower than expected (4). It seems to be very important to define new catalytic formulations.

In a previous study (5), model phosphate catalysts with a mixed valency enabled us to understand the catalytic activity for the mild oxidation of propane. The same approach has been followed in the present investigations. We report the catalytic properties of nickel iron phosphates for the selective oxidation of hydrogen sulfide to sulfur. Their performance is compared to those of unsupported iron and chromium oxides and mixed iron–chromium oxides (6).

EXPERIMENTAL

Catalysts

A polycrystalline $Ni_3Fe_4(PO_4)_6$ sample, referred to as $Ni_3Fe_4(PO_4)_6$ (SS), was prepared according to the solid–solid method as described in the literature (7). First, Fe_2O_3, $(NH_4)_2HPO_4$ and NiO were mixed in an agate mortar in the appropriate ratio; the mixture was then heated in a platinum crucible at about 673 K in air for at least 3 h to eliminate NH_3 and H_2O. In a second step, the product was finely ground and heated in air at 1223 K for 12 h.

To obtain catalysts with a high specific area, another method was used: stoichiometric proportions of $Ni(CH_3COO) \cdot 2H_2O$, $Fe_2(NO_3)_3 \cdot 9H_2O$, and $(NH_4)_2HPO_4$ precursors were dissolved in water at room temperature. To avoid precipitation, the acidic pH of the solution was maintained by addition of nitric acid. The resulting solution was evaporated and stirred at 353 K for 24 h; the obtained paste was dried at 383 K for 12 h and then calcined for 4 h at the

[1] To whom correspondence should be addressed at present address: Laboratoire de Réactivité de Surface, Université Paris VI, 4 place Jussieu, Tour 54/55, 75252 Paris Cédex 05, France. E-mail: costenti@ccr.jussieu.fr.

0021-9517/99 $30.00

following temperatures: 673, 723, 773, 823, 873, 923, 973, 1023, or 1123 K. The obtained solids were referred to as $Ni_3Fe_4(PO_4)_6$ (AS-T), where AS is aqueous solution and T is the calcination temperature.

Iron and chromium oxides were provided by Procatalyse and corresponded to α-Fe_2O_3 and α-Cr_2O_3 phases, respectively. Mixed iron–chromium oxide was prepared from the corresponding citrates in order to obtain high specific area samples. Iron and chromium nitrates ($Fe(NO_3)_3 \cdot 9H_2O$) and $Cr(NO_3)_3 \cdot 9H_2O$) were dissolved in 40 mL of water in the appropriate ratio to obtain Cr/Fe = 0.5. Citric acid was dissolved in about 30 mL of water and slowly added to the nitrate solution. The mixture was heated to 343 K and stirred for 3 h. After drying the solid product at 363 K overnight, it was calcined in air at 773 K.

Characterization

The specific area of the prepared catalyst samples was determined with a Micromeritics Model 2000 sorptiometer. The samples were outgassed at 673 K for 2 h before adsorption of N_2. The area was calculated using the BET method.

X-ray powder diffraction patterns of $Ni_3Fe_4(PO_4)_6$ samples were registered using Cu $K\alpha$ radiation and indexed according the crystallographic symmetry and parameters deduced from the single crystal studies (7).

The studied compounds were also characterized by powder Mössbauer spectroscopy using a constant acceleration spectrometer with a ^{57}Co source in a Rh matrix. The isomer shift (IS) values are given with respect to that of α iron oxide at room temperature.

Catalytic Tests

The catalytic tests were carried out in a fixed bed continuous flow quartz microreactor operating at atmospheric pressure at 503 K. Fifty-milligram granules, in the range of 0.4–1 mm, diluted in 350 mg of quartz powder was used. The reactor was heated externally by a tube furnace; the temperature of the catalyst bed was maintained to within ± 1 K of the required value and controlled by a thermocouple near the wall of the quartz tube.

The catalyst was heated directly to 503 K in a flow of reactants. The feed was a mixture of H_2S–O_2 diluted with N_2, with the following ratio: 1.2% H_2S, 1% O_2, 97.8% N_2. The total flow rate was 47 mL min^{-1} (W/F = 0.4 g · h mol^{-1}). The quartz or Teflon lines of the catalytic test unit were heated to avoid condensation of water or sulfur. The reaction products were separated into water and sulfur, which were trapped at room temperature, and gaseous products.

The inlet and outlet gases were analyzed online by gas chromatography using a Varian 3400 CPG apparatus equipped with a FPD detector and a 25-m Porapak Q column. The minimum detectable amount of H_2S and SO_2 is 70 ppm. The conversion of the hydrogen sulfide and sulfur selectivity were calculated using the equations

$$\text{Conversion (\%)} = (\text{moles of hydrogen sulfide reacted})/(\text{moles of hydrogen sulfide fed}) * 100\% \text{ and}$$

$$\text{Sulfur selectivity (\%)} = (\text{moles of hydrogen sulfide reacted} - \text{moles of sulfur dioxide produced})/(\text{moles of hydrogen sulfide reacted}) * 100\%.$$

BET

The specific areas of Fe_2O_3 and Cr_2O_3 and Fe/Cr = 0.5 oxides are 22, 42, and 78 $m^2\ g^{-1}$, respectively.

BET measurements revealed that the $Ni_3Fe_4(PO_4)_6$ (SS) sample, which was very well crystallized, therefore has a very low specific area ($<1\ m^2\ g^{-1}$). As expected, the samples prepared from aqueous solution exhibited higher surface areas, reaching 90 $m^2\ g^{-1}$ for $Ni_3Fe_4(PO_4)_6$ (AS-673). The specific area decreased as the temperature of calcination increased (Fig. 1). The decrease is very rapid above 773 K and corresponds to the beginning of crystallization of the $Ni_3Fe_4(PO_4)_6$ phase as shown below.

XRD

Comparisons with ASTM files confirmed that iron and chromium simple oxides are α-oxides, whereas in iron–chromium oxide, iron oxide is present in the maghemite form (γ-Fe_2O_3). The presence of chromium in iron oxide would stabilize this latter phase at the expense of the

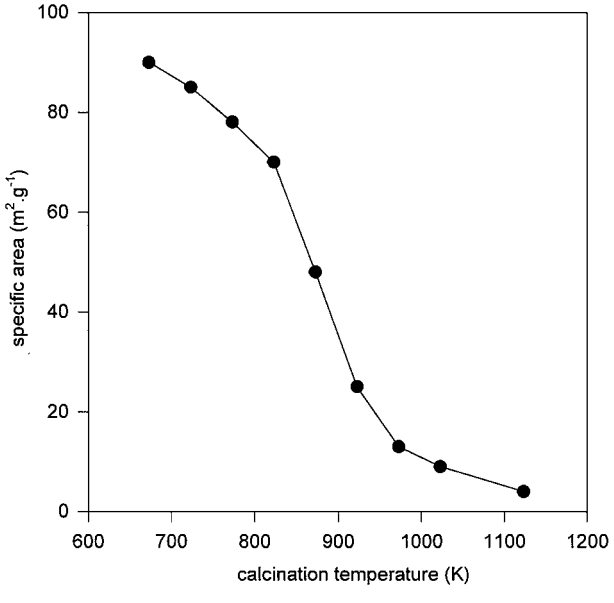

FIG. 1. Specific area versus calcination temperature of $Ni_3Fe_4(PO_4)_6$ (AS-T) samples.

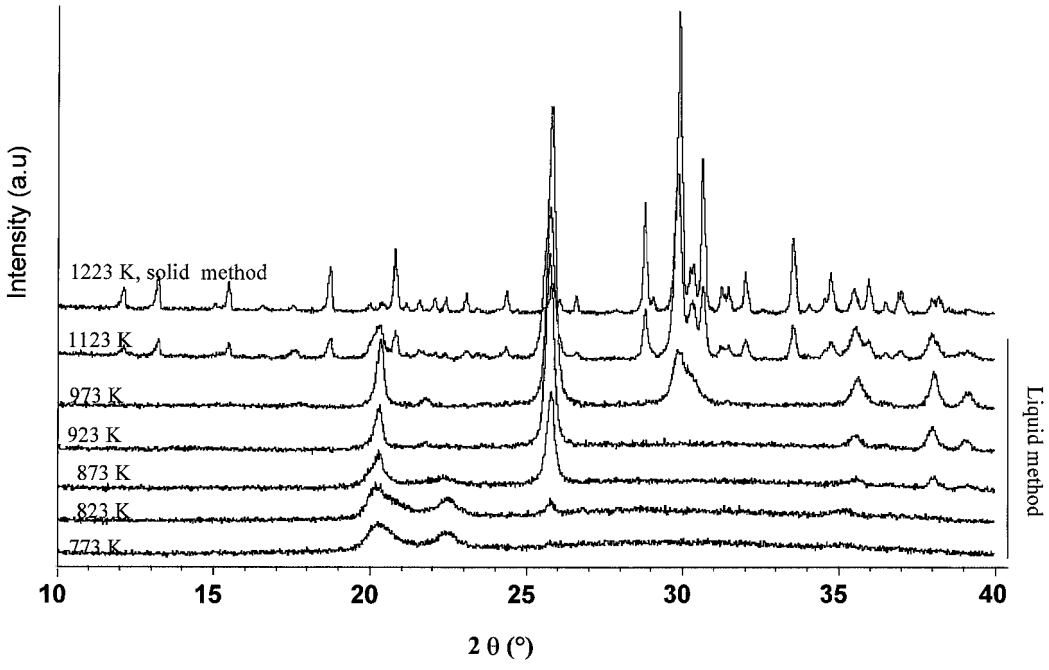

FIG. 2. X-ray diffraction pattern of $Ni_3Fe_4(PO_4)_6$ samples. —solid–solid preparation method, $T_{calcination} = 1223$ K; —solution preparation method, $T = 773$, 823, 873, 923, 973, and 1123 K.

α phase (6). The presence of $FeCr_2O_4$ was also detected, iron being indeed divalent. Consequently, in the mixed iron–chromium oxide, the concomitant presence of Fe^{3+} and Fe^{2+} species is expected. (8).

XRD characterizations (Fig. 2) show that the $Ni_3Fe_4(PO_4)_6$ (SS) sample is very well crystallized, implying that it has a very low specific area, as seen above. The $Ni_3Fe_4(PO_4)_6$ structure is well known and has been described elsewhere (7). It exhibits a triclinic 3-D framework involving trivalent iron and divalent nickel ions. Two crystallographically independent iron atoms in general position (degeneracy of 2) are octahedral coordinated and built-up bioctahedral units. Ni^{2+} cations are also located at two independent crystallographic sites, but they present two kinds of coordination: octahedral and trigonal bipyramidal (Fig. 3) corresponding to respective degeneracy of 1 and 2. Finally, the positions of the metallic atoms lead to four iron and three nickel atoms per unit cell.

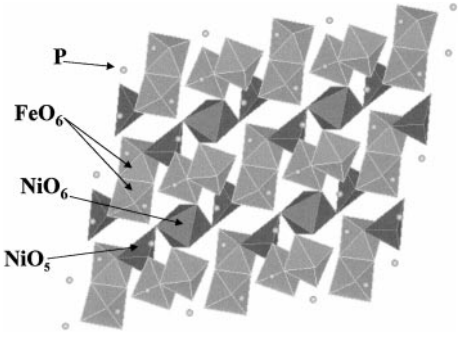

FIG. 3. Projection of $Ni_3Fe_4(PO_4)_6$ structure along [100].

According to El Kira *et al.* (7), the pure $Ni_3Fe_4(PO_4)_6$ compound is very difficult to prepare. Because of the low symmetry (triclinic), one cannot completely reject from the X-ray powder data the possibility to have prepared solid solution $Ni_{3-x}Fe^{II}_xFe^{III}_4(PO_4)_6$ or mixing of $Ni_3Fe_4(PO_4)_6$ (major phase) and $Fe_7(PO_4)_6$ (minor phase). Low amounts of the simple oxides NiO and P_2O_5 are also undetectable by X-ray diffraction.

Samples prepared by the aqueous solution method are amorphous up to a calcination temperature of 773 K. The sample calcined at 773 K (Fig. 2) exhibits two diffraction lines, corresponding to the (012) and (021) indexation of the $Ni_3Fe_4(PO_4)_6$ phase. At higher calcination temperatures (Fig. 2), samples become increasingly crystalline, and the resulting crystalline phase corresponds to the $Ni_3Fe_4(PO_4)_6$ compound. Nevertheless, the relative intensities of the diffraction lines depend on the preparation method: the morphology of the $Ni_3Fe_4(PO_4)_6$ (SS) and (AS-T) is, thus, different. Particle sizes have been compared from the Scherrer equation: the size varies between 120 and 600 Å for AS-T samples, whereas, in SS sample, the particles size reaches 2400 Å.

No modification of the X-ray powder diffraction patterns was detected after the catalytic tests.

Mössbauer

Three $Ni_3Fe_4(PO_4)_6$ samples were characterized before and after the catalytic reaction by Mössbauer spectroscopy:

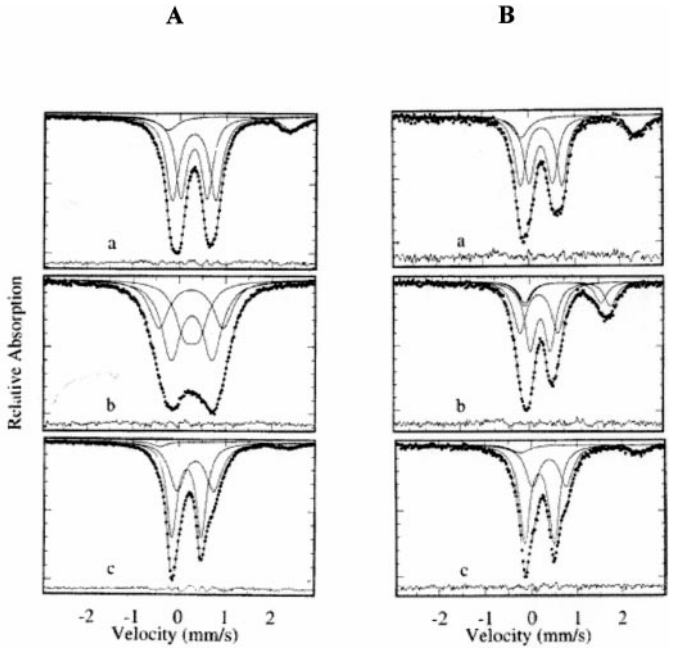

FIG. 4. Mössbauer spectra before (A) and after (B) catalytic test. (a) $Ni_3Fe_4(PO_4)_6$ (SS); (b) $Ni_3Fe_4(PO_4)_6$ (AS-773); (c) $Ni_3Fe_4(PO_4)_6$ (AS-1123).

$Ni_3Fe_4(PO_4)_6$ (SS), (AS-1123), and (AS-773). After catalytic reaction, samples were cooled to room temperature under reactional flow. Then, Mössbauer spectra were registered at room temperature without keeping samples separated from air. The Mössbauer spectra of the compounds (Fig. 4) indicated the occurrence of pure electric quadrupolar interactions and were fitted using the MOSFIT program (9).

Samples before catalytic reaction. It is concluded from the Mössbauer spectra that Fe^{3+} species are at octahedral sites, and, consequently, Ni^{2+} species occupy the two divalent crystallographic sites of the isostructural $Fe_7(PO_4)_6$ compound (10). These latter sites correspond to an octahedral and a trigonal pyramidal one. This five-coordination is quite unusual for Ni^{2+}: according to El Kira *et al.* (7), the competition between Ni^{2+} and Fe^{3+} for six-coordinated sites is, to some extent, detrimental to Ni^{2+}. Although the theoretical oxidation state of iron should be Fe^{3+} in $Ni_3Fe_4(PO_4)_6$ before the catalytic test, 12% of Fe^{2+} species are detected in $Ni_3Fe_4(PO_4)_6$ (SS). This divalent charge is characterized by the high values of the isomer shift and of the quadrupole splitting (QS): 1.14 and 2.71 mm s^{-1} respectively (Table 1). To respect the electroneutrality and compensate the presence of a small amount of Fe^{2+}, one can propose two hypotheses: (i) a minor part of Ni may be in the Ni^{3+} oxidation state and localized at a trivalent six-coordinated site of the structure. Nickel *K*-edge XANES studies are in progress to check this point. (ii) The preparation may not be single phased with the simultaneous presence of $Ni_3Fe_4(PO_4)_6$ and $Fe_7(PO_4)_6$ (plus NiO and P_2O_5) or with the formation of the solid solution $Ni_{3-x}Fe^{II}_xFe^{III}_4(PO_4)_6$ (plus NiO). As mentioned above, X-ray powder characterizations did not enable us to come to a conclusion regarding this point.

$Ni_3Fe_4(PO_4)_6$ (AS-1123) and $Ni_3Fe_4(PO_4)_6$ (AS-773) contain only 0 and 4% of Fe^{2+} species, respectively. Moreover, Fig. 4 and Table 1 show that the width of the Mössbauer signal (see Γ in Table 1) depends on the calcination temperature: the less crystalline the sample, the less symmetric the environment of the iron species. It must be also noticed that, in the $Ni_3Fe_4(PO_4)_6$ (AS-773) sample, the size of crystallites is 120 Å only about (from analysis of the XRD line broadening): such small particles can lead to quadrupolar splitting different from that expected from the perfect tridimensional crystalline matrix. It may thus explain the presence of three Fe^{3+} local environments (Table 1) instead of the two theoretical crystallographic sites observed in the crystalline sample.

Samples after catalytic reaction. In all cases, the proportion of Fe^{2+} species is increased after the catalytic reaction (Fig. 4B, Table 1). After the catalytic test, $Ni_3Fe_4(PO_4)_6$ (SS) contained 21% Fe^{2+}, whereas $Ni_3Fe_4(PO_4)_6$ (AS-1123) and $Ni_3Fe_4(PO_4)_6$ (AS-773) contained 10 and 31%, respectively. Since the measurements were not performed under *in situ* conditions or, at least, keeping samples separated from air, partial reoxidation of the surface may have occurred. The

TABLE 1

Mössbauer Data Obtained before and after Catalytic Reaction of $Ni_3Fe_4(PO_4)_6$ (SS) and $Ni_3Fe_4(PO_4)_6$ (AS-773) and (AS-1123) Samples

Synthesis method	Reaction	δ (mm s^{-1})	Γ (mm s^{-1})	Δ (mm s^{-1})	Fe oxidation state	%
Solid method	Before	0.43	0.29	0.57	3+	40
		0.43	0.33	0.94	3+	48
		1.14	0.48	2.71	2+	12
	After	0.38	0.28	0.50	3+	38
		0.40	0.28	0.90	3+	42
		1.22	0.42	2.53	2+	20
Solution method (AS-773)	Before	0.38	0.54	0.30	3+	26
		0.38	0.48	0.88	3+	45
		0.37	0.49	1.38	3+	28
	After	0.42	0.36	0.58	3+	36
		0.38	0.44	1.09	3+	33
		1.09	0.44	2.23	2+	14
		1.23	0.44	2.51	2+	16
Solution method (AS-1123)	Before	0.28	0.26	0.64	3+	54
		0.47	0.40	0.79	3+	42
		1.09	0.34	2.81	2+	4
	After	0.28	0.28	0.64	3+	58
		0.50	0.36	0.74	3+	32
		1.18	0.50	2.62	2+	10

Note. δ, isomer shift; Γ, line width; Δ, quadrupolar splitting.

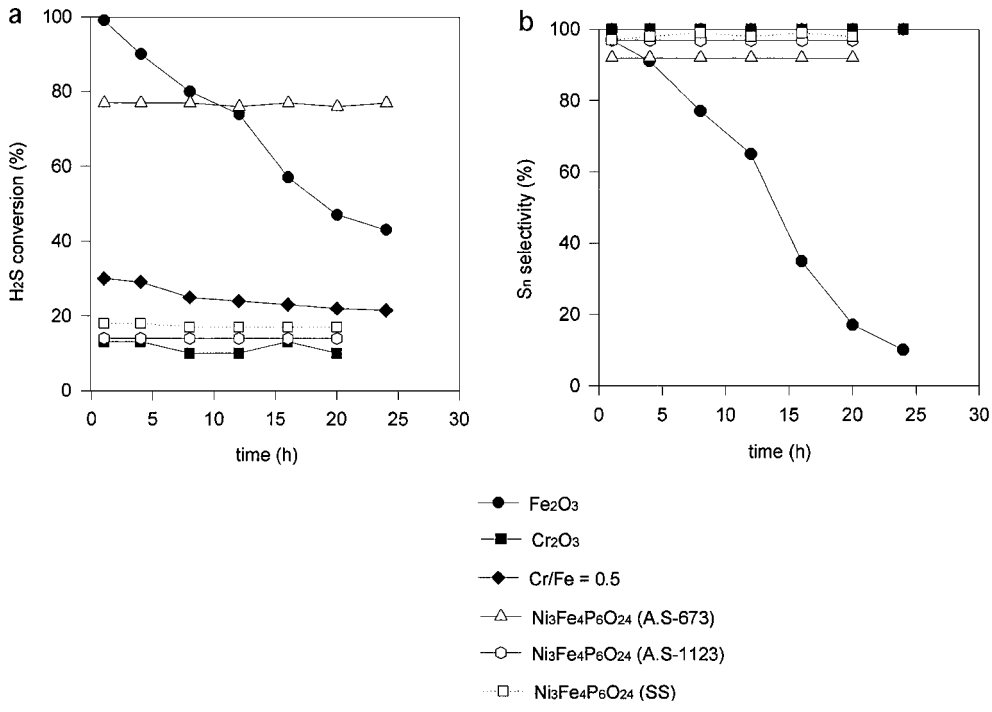

FIG. 5. (a) H_2S conversion versus time for α-Fe_2O_3, α-Cr_2O_3, and mixed oxide Fe/Cr = 0.5 and for $Ni_3Fe_4(PO_4)_6$ (SS), (AS-673), and (AS-1123) samples; (b) S_n selectivity versus time for α-Fe_2O_3, α-Cr_2O_3, and mixed oxide Fe/Cr = 0.5 and for $Ni_3Fe_4(PO_4)_6$ (SS), (AS-673), and (AS-1123) samples.

amounts of divalent iron species found by this procedure in the three samples may minimize the reduction phenomenon which has obviously occurred during reaction.

REACTIVITY

All samples were tested under similar conditions. Figure 5a shows that the initial conversion of Fe_2O_3 is very high but decreases sharply with time on stream, while the S_n selectivity drops rapidly as well (Fig. 5b). According to Berben (3), deactivation would be related to iron sulfide formation, which could also enhance O_2 consumption and increase thus SO_2 formation. Over chromium oxide, conversion is also quite low (12%) but remains more stable over time. The mixed Cr/Fe = 0.5 oxide leads to a better selectivity, but its activity appears rather low, considering its surface area.

All the $Ni_3Fe_4(PO_4)_6$ samples are active for H_2S oxidation. Their conversion and sulfur selectivity remained stable over time with no deactivation observed up to 24 h on stream (Figs. 5a and 5b). Moreover, their S_n selectivity is very high, always above 90%. More precisely, the H_2S conversion of $Ni_3Fe_4(PO_4)_6$ (SS) is 17%, with 97% of sulfur selectivity. $Ni_3Fe_4(PO_4)_6$ (AS-T) samples give higher conversion results under the same reactional conditions in relation to their higher specific area (Fig. 6). For instance, the H_2S conversion reaches 76% for $Ni_3Fe_4(PO_4)_6$ (AS-673).

DISCUSSION

Considering its very low specific area, $Ni_3Fe_4(PO_4)_6$ (SS) has a very good activity. In comparison, for the nonsupported mixed iron chromium oxide (Cr/Fe = 0.5), the composition of which was optimized to obtain the best activity in this system (6), H_2S conversion is only about 23% after 20 h in spite of its high specific area (78 $m^2\,g^{-1}$). Moreover,

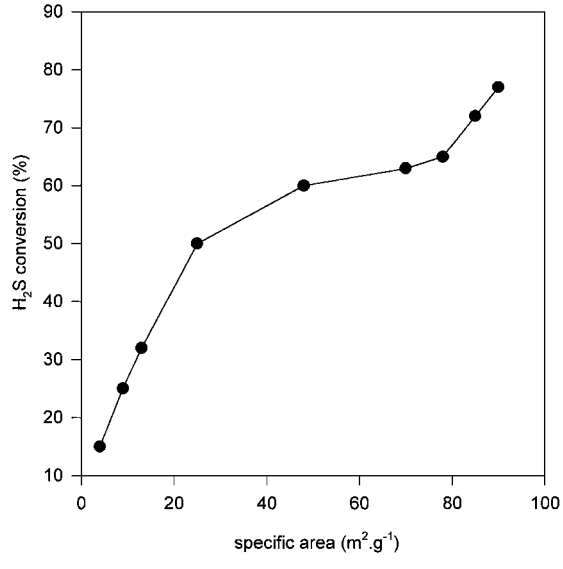

FIG. 6. H_2S conversion versus specific area.

in contrast to the simple iron oxide, no deactivation occurs under the conditions used, and the S_n selectivity, which is a primordial point, is about 97%. Taking into account that the main feature of this process is to get high S_n selectivity, this value appears very promising, even though better S_n selectivity is obtained with Cr/Fe = 0.5 mixed oxide (100%). The main advantage of our new performant system compared to iron chromium mixed oxides is to eliminate toxicity due to chromium. Moreover, this result indicates that, for the mild oxidation of H_2S to sulfur, the association of iron with another element, here nickel, leads to better performance than over Fe_2O_3 alone.

Results obtained over $Ni_3Fe_4(PO_4)_6$ (AS-T) samples are obviously better in terms of H_2S conversion, due to their higher specific area. Furthermore, the S_n selectivity remains high (>90%), even though it is slightly decreased compared to that of $Ni_3Fe_4(PO_4)_6$ (SS). Therefore, the catalytic performance of these new catalytic systems appears to be very promising.

Nevertheless, the increase in the H_2S conversion is not only relative to the specific area of the catalyst. If one considers the specific activity, defined as the moles of H_2S reacted per unit of surface (Fig. 7), then it appears that it does not vary for samples calcined between 673 and 823 K, whereas at higher temperature, there is a constant increase. In other words, the specific activity remains constant so long as the samples are amorphous and increases as they become increasingly crystallized. Results for $Ni_3Fe_4(PO_4)_6$ (SS) are imprecise because of its very low specific area. Supposing that it is less than 1 $m^2\,g^{-1}$ leads to a specific activity higher than 15, i.e., much higher than that of the $Ni_3Fe_4(PO_4)_6$ (AS) samples calcined at the highest temperature (1123 K). This is relating to the better crystallinity of the latter: Fig. 2 clearly shows that the $Ni_3Fe_4(PO_4)_6$ (AS-T) samples have a less well-organized structure even when $T = 1123$ K. These features demonstrate that the mild oxidation reaction of H_2S into sulfur is structure sensitive. Attempts to correlate the activity results to particle sizes ranges, evaluated from the (012) and (021) crystallographic planes, failed. It can be noticed that these two planes, developed at low calcination temperature, become minor in the well-crystallized samples ($T > 973$ K) compared to the plane (212) ($2\theta = 30^\circ$). Actually, activity results could thus be more sensitive to the nature of the plane preferentially exposed.

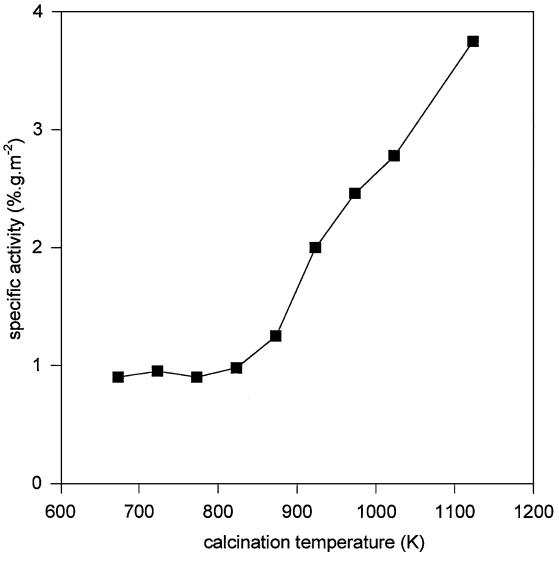

FIG. 7. Specific activity versus calcination temperature.

Mössbauer results underline the importance of the Fe^{2+}/Fe^{3+} mixed valency toward the H_2S selective oxidation reaction. A similar result was recently reported by Davydov *et al.* (11) on the Fe_2O_3 system. The electronic exchanges leading to the establishment of such mixed valency are facilitated when the relative positions of the active sites are structurally optimized inside the framework: the configuration into bioctahedral units in the well-crystallized sample (Fig. 3) seems favorable for such electronic exchange. Moreover, such active bioctahedral units should be included in a flexible three-dimensional structure to allow the relaxation of such electronic effects. Thus, the participation of the whole structure is expected. The presence of a second element probably promotes electronic exchange. In order to evaluate its influence, and since the Ni crystallographic sites can be substituted easily by several other divalent cations, studies are in progress to compare the catalytic activity of isostructural compounds.

The results obtained, in particular the structure sensitivity of the H_2S oxidation, enable comparison with the mild oxidation reaction of light hydrocarbon compounds. Since the Mars and van Krevelen mechanism (12) is involved for the latter reactions, it is also suggested for H_2S mild oxidation, in agreement with Zhenglu *et al.* (13). Bioctahedral units, present in VPO catalysts, also contributed to their reactivity toward *n*-butane mild oxidation (5). The establishment of a mixed valency V^{4+}/V^{5+} or Mo^{5+}/Mo^{6+} (14–16) also appears to be very important. In particular, it was concluded that the relative organization of the active sites, in the form of polynuclear limited sized sites (17), enhances electronic exchange. Such results have never been reported for H_2S mild oxidation and should be applied to define improved catalysts.

CONCLUSION

This study showed that a model catalyst can develop good intrinsic activity versus H_2S mild oxidation. The new method of preparation resulted in samples with higher specific areas and better catalytic performance. This new catalyst, with stable S_n selectivity >90%, could thus be considered as very promising, even if, up to now, the synthesis cost could appear as the limiting factor for its industrial development. Attempts to deposit this active phase on a support are in progress.

This study underlines the structure-sensitive character of the reaction. Our results allow a better understanding of the mechanism and the active phase. Moreover, since many other isostructural iron phosphate compounds are available, the comparisons of their respective performances toward this reaction will probably enable us to evaluate the influence of the nature of the elements on catalytic activity.

ACKNOWLEDGMENTS

The authors thank ADEME for financial support and Procatalyse for providing chromium and iron oxides.

REFERENCES

1. Estep, J. W., Mc Bride, G. T., and West, J. R., *in* "Advances in Petroleum Chemistry and Refining," Vol. 6, Chapter 7, p. 315. Interscience, New York, 1962.
2. Lagas, I. A., Borboom, J., Berben, P. H., Geus, J. W., European Patent application 02 4200 6, 1985.
3. Berben, P. H., thesis. Utrecht, the Netherlands, 1992.
4. "Les techniques de désulfuration des procédés industriels," ADEME Report, XXVIth section, 1998.
5. Savary, L., thesis. Caen, France, 1996.
6. Pieplu, A., thesis. Caen, France, 1994.
7. El Kira, A., Gerardin, R., Malaman, B., and Gleitzer, C., *Eur. J. Solid State Inorg. Chem*. **t.29**, 1119 (1992)
8. Fattakhova, Z. T., Ukarshii, A. A., Shiryaev, P. A., and Berman, A. D., *Kinet. Catal.* **27**, 766 (1986).
9. Teillet, J., and Varret, F., unpublished MOSFIT program.
10. Gorbunov, A., Maksimov, B. A., Kabalov, Y. K., Ivaschenko, A., Mel'nikov, O. K., and Belov, N. V., *Dokl. Akad. Nauk. SSSR* **254c**, 873 (1980).
11. Davydov, A., Chuang, K. T., and Sanger, A. R., *J. Phys. Chem. B* **102**, 4745 (1998).
12. Mars, P., and van Krevelen, D. W., *Chem. Eng. Sci.* **3**, 41 (1954).
13. Zhenglu, P., Weng, H. S., Han-Yu, F., and Smith, J. M., *AIChE J.* **30**, 1021 (1984).
14. Nguyen, P. T., and Sleight, A. W., *J. Solid State Chem*. **122**, 259 (1996).
15. Herrmann, J. M., and Védrine, J. C., *Appl. Catal.* **76**, 209 (1991).
16. Savary, L., Costentin, G., Maugé, F., Lavalley, J. C., El Fallah, J., Studer, F., Guesdon, A., and Ponceblanc, H., *J. Catal.* **169**, 287 (1997).
17. Costentin, G., Savary, L., Lavalley, J. C., Borel, M. M., and Grandin, A., *Chem. Mater.* **10**, 59 (1998).